




Molecular dynamics simulation of the formation of bimetallic core-shell nanostructures with binary Ni–Al nanoparticle quenching

Sergei Bogdanov¹, Vladimir Samsonov¹, Nickolay Sdobnyakov^{1,*} , Vladimir Myasnichenko¹, Igor Talyzin¹, Kseniya Savina¹, Valentin Romanovski², and Andrei Kolosov¹

¹General Physics Department, Tver State University, Tver, Russia 170002

²Department of Materials Science and Engineering, University of Virginia, Charlottesville, VA 22904, USA

Received: 2 April 2022

Accepted: 21 June 2022

Published online:
11 July 2022

© The Author(s), under exclusive licence to Springer Science+Business Media, LLC, part of Springer Nature 2022

ABSTRACT

Employing isothermal molecular dynamics, we simulated the self-assembly of core-shell nanostructures in the course of quenching binary Ni–Al nanoparticles (NPs) with initially homogeneous distributions of both components. The process of quenching was reproduced via the uniform rapid cooling of initial configurations from temperatures of 1000 K down to 0.001 K. To increase the reliability of the simulation results, we used two independently developed computer programs (our own and the well-known open program LAMMPS) in conjunction with the tight-binding potential (TBP) model and the embedded atom method (EAM). Simulations employing both force fields predict the self-assembly of the core-shell nanostructures whose shells consist of Al atoms. However, involving TBP predicts the formation of more perfect Ni@Al structures, in which the central area (core) consists almost completely of Ni atoms, whereas EAM simulations predict formation of a more complex integral structure Ni–Al@Ni@Al. In the last case, the first (outer) monolayer also entirely consists of Al atoms, the second—of Ni atoms, while the core is comprised of both types of atoms. At the same time, the core is enriched by Ni atoms. It is concluded that the spontaneous surface segregations of Al atoms should be considered as the main driving force for the formation of the core-shell structures during quenching of Ni–Al NPs with initially homogeneous distributions of components.

Handling Editor: N. Ravishankar.

Address correspondence to E-mail: nsdobnyakov@mail.ru

<https://doi.org/10.1007/s10853-022-07476-2>

Introduction

Ni–Al alloys are widely used in many technologies [1–3]. Five different intermetallic phases have been identified in such alloys: NiAl₃, Ni₂Al₃, NiAl, Ni₅Al₃, and Ni₃Al [4], each demonstrating different degrees of stability. However, at room temperature, the highest stability is exhibited by the equiatomic composition NiAl. Since the 1990s, great interest has been shown in binary Ni–Al nanoparticles (NPs), including bimetallic NPs having partially separated (segregated) components. Such nanoalloys include, in particular, Ni@Al and Al@Ni core–shell nanostructures. Here, the first component (before the @ symbol) corresponds to the core, while the second refers to the NP shell. Such nanostructures can be obtained by both one-step and two-step synthesis approaches. Thus, in [5], the Al@Ni magnetic pigment NPs were obtained using the galvanic displacement reaction. In [6], the first step corresponded to the synthesis of Al NPs, on which Ni atoms were then chemically deposited.

In [7], Ni–Al intermetallic compounds from Ni and Al powders were obtained by thermal explosion. The effect of the molar ratio of Ni to Al in the feedstock on the phases, microstructure and microhardness of the final materials was studied. The results show that a single phase of NiAl was obtained with a composition corresponding to the ratio of mole fractions $x_{Ni} : x_{Al} = 1:1$. However, when the molar ratio of Ni to Al was increased to 2:1, the product resulting from the explosion consisted of Ni₃Al and NiAl, in which the NiAl phase dominated. As well as appearing in a smaller quantity, the Ni₃Al phase had irregular morphology, mainly along the grain boundary. With a further increase in the molar ratio of Ni to Al to 3:1, the microstructures of the material became even more diverse.

Taking into account the high-temperature strength of bulk Ni–Al alloys due to their low density, high melting point, high thermal conductivity, excellent resistance to acid/alkali corrosion, as well as good oxidation resistance at elevated temperatures [1–3], similar properties can be expected from Ni–Al nanoalloys and related nanostructured materials. It is additionally noted that Al NPs with a shell composed of Ni atoms have improved characteristics when used as a solid fuel component [8, 9]. In particular, such a shell eliminates the combustion instability effect.

Since experimental studies of structural transformations in NPs, including the structural stability of Ni–Al nanoalloys, are associated with some difficulties, starting from the 2000s, Ni–Al nanoalloys have been increasingly studied using atomistic simulation methods. In particular, in [10], structural transformations in Ni@Al NPs of 5.6 nm in size (number of atoms $N = 5636$) were studied by using molecular dynamics (MD) simulation. Here, it was shown that, at a temperature of 1000 K, the NP core–shell structure is destroyed—that is, transformed into NPs having uniform component distributions. The indicated transition temperature corresponds to a minimum on the V-shaped temperature dependence of the potential (cohesive) term u into the specific (per atom) internal energy. The thermodynamic and structural properties of Al@Ni and Ni@Al NPs were studied in more detail in a recent work [11]. Both the MD simulations [10, 11] used the LAMMPS program and the embedded atom method (EAM).

In [12, 13], we proposed and confirmed in MD experiments a hypothesis about the relationship between the stability/instability of core-shell nanostructures and the spontaneous surface segregation of one of the components. In accordance with this hypothesis, one of the two alternative nanostructures A@B and B@A will be stable whose shell corresponds to the component that spontaneously segregates to the surface of binary NPs A–B with the initial uniform distributions of components. In our recent paper [14], the conclusion reached in [12] was revised. In particular, it was acknowledged that the concepts of stability and instability of core-shell bimetallic NPs are somewhat conventional; that is to say, it is more correct to talk about the greater or lesser stability of one of the two alternative abovementioned nanostructures. Thus, a structure may be considered as more stable if it corresponds to a longer lasting stability at a given temperature. In particular, it was found that at high temperatures above the melting point of Al, Ni@Al NPs demonstrated higher stability, which was consistent with our initial hypothesis. In fact, both atomistic and thermodynamic simulations predict the segregation of Al atoms to the surface of Ni–Al NPs. The hypothesis about the relationship between the stability/instability of core-shell nanostructures and the spontaneous surface segregation is also confirmed for bimetallic nanostructures based on other metals, both according to the results of our MD experiments and those given in

[15]. However, at low temperatures, it is not bimetallic Ni@Al NPs, but Al@Ni NPs that demonstrate higher stability since the shell of Ni atoms behaves like a solid crust that inhibits the diffusion of Al atoms to the surface of such NPs and, accordingly, prevents the destruction of the core-shell nanostructure.

The works mentioned above [10–15], as well as a detailed review [16], are devoted to MD simulation of structural transformations in prefabricated core-shell bimetallic nanostructures – in particular, to simulating the melting of such nanostructures. However, the question concerning the possible self-assembly of core-shell nanostructures in NPs having an initially uniform distribution of components, as well as the conditions necessary for such self-assembly, remains open. It is quite evident that one of these conditions affecting the processes of structure formation in binary nanoparticles consists in the surface segregation of one of the components. Segregation in bimetallic NPs was considered in a recent review [17], including the surface segregation in nickel-containing bimetallic NPs. However, aluminum-based bimetallic NPs were not considered in this review.

Although the MD results presented in the present work refer to binary Ni–Al NPs, similar structural transformations should also be observed upon quenching of binary NPs consisting of other metals characterized by pronounced surface segregation of components. In a recent work [18], the importance of studying the regularities of the crystal structure transformations in metal NPs when engineering the crystalline phase was discussed. The present work is devoted to the equally important problem of engineering the integral structure of binary metal NPs: elucidation of regularities and mechanisms of the self-assembly of various types of metal core-shell nanostructures.

Methods

In order to elucidate the conditions, regularities, and mechanisms of the formation of bimetallic nanostructures by the quenching method, our MD experiments reproduced the quenching process, i.e., rapid cooling of Ni–Al NPs with an initial uniform distribution of components. The main objects of study were NPs of equiatomic composition containing 5000 atoms, i.e., 2500 Ni atoms and 2500 Al atoms

(the NP size is of about 5 nm). However, larger Ni–Al NPs with different component ratios were also simulated for comparison. As noted in [4], although the equiatomic ratio of the components corresponds to a stable bulk phase, at the same time, it does not correspond to the regions of the phase diagram where the formation of intermetallic compounds is most characteristic. In addition, the 1:1 component ratio and those close to it are most often used in non-chemical (dry) methods for the synthesis of bimetallic NPs – for example, in the method of the electric explosion of wires (EEW) [19].

Since Ni–Al NPs are characterized by a significant difference in the binding energies of the components, a dimensional mismatch of atoms and a concomitant tendency to form intermetallic compounds, in order to increase the reliability of the results of MD simulation, we used two different force fields corresponding to the tight-binding potential (TBP) [20] and to the embedded atom method (EAM) with the parametrizations proposed for Ni and Al in [21]. Some additional information on engaged interatomic potentials is presented in Appendix.

TBP [20] was initially proposed to describe interatomic interaction in both single-component and binary metal nanosystems. In particular, an integrated approach (joint use of MD and Monte Carlo methods) allowed sufficient testing to determine a number of thermodynamic characteristics, including temperatures and melting heats [22]. The stability of bimetallic NPs was also evaluated [23]. In addition, we can note the use of TBP in a computer experiment for the synthesis of bimetallic Ni–Cu NPs, whose results are in good agreement with the experimental results on the synthesis of bimetallic NPs by the method of exothermic combustion in solutions [24, 25]. The main problem with the use of TBP is reduced to the appropriate selection of parameters describing the interaction between Ni and Al atoms. In the present work, these parameters were estimated by using the Lorentz-Berthelot rule, whose application is described, for example, in [26]. The algorithm proposed and verified in [21] allows the generation of a potential for the Ni–Cu system using the parametrizations proposed for the components was also used in the present work.

It is quite evident that the results of quenching, i.e., of rapid cooling, will depend on the initial NP temperature. We chose the pre-relaxation (annealing) temperature equal to 1000 K, which is lower than the

macroscopic melting point of nickel (1727 K [27]) but higher than the melting point of aluminum (933.5 K [27]). Such a ratio relates to single-component Ni and Al NPs containing both 2500 and 5000 atoms (Table 1).

At initial temperatures below the melting temperature of both components, quenching does not lead to a noticeable change in the initial structure of binary NPs with an initial uniform distribution of Ni and Al atoms. The initial configurations of binary Ni–Al NPs were either spherical or cubic (Fig. 1). The simulation results do not show any dependence on the initial shape of NPs.

Results

Results obtained by employing TBP

Figure 2 shows the appearance and central cross section of the final configuration obtained by cooling an initial cubic NPs (Fig. 1b) having a random distribution of components. Cooling from 1000 to 0.01 K was carried out at a rate of 0.06 K/ps. Compared with the usual standards, this rate is very high. However, in MD simulation of the solidification of metal NPs, higher cooling rates of the order of 1 K/ps are typically used. In particular, in [10], the solidification of Ni–Al nanodroplets containing 5636 atoms (3620 Ni atoms and 2016 Al atoms) occurred upon cooling rates of 6.5 K/ps and 0.13 K/ps. In the first case, an amorphous structure was formed, whereas in the second case the formed structure was crystalline. Thus, the selected cooling rate should provide the necessary conditions for forming a quasiequilibrium structure of NPs by quenching. This cooling rate corresponds to $50 \cdot 10^6$ MD simulation steps (one step

corresponds to the 1 fs time step commonly used in contemporary MD experiments). So, the whole time of quenching t_{qu} was 50 ns.

It is shown in Fig. 2 that, as a result of quenching, a sufficiently perfect Ni@Al nanostructure in terms of the degree of component segregation was formed, whose shell is represented by two or three monolayers of Al atoms. As expected, both individual Al atoms and clusters of several Al atoms are present in the NP core shown in Fig. 2. For comparison, Fig. 3 and 4 present the configurations of a truncated octahedron (fcc structure) and an icosahedron, respectively, which were both obtained by short-term (10 ps) relaxation of the initial Ni@Al nanostructures in the form of these polyhedra. As can be seen from Fig. 3b and 4b, the nuclei in the relaxed nanostructures are completely represented by Ni atoms.

The ratio R^2/t_{qu} of the square particle radius $R^2 = 6.25 \text{ nm}^2$ to the quenching time $t_{qu} = 50 \text{ ns}$ may be considered as a loose but reasonable evaluation of the interdiffusion coefficients D_i of components in binary Ni–Al NPs with the initially uniform distribution of components. Such an evaluation predicts a relevant value of $10^{-10} \text{ m}^2/\text{s}$. Really, structural and transport properties of NPs should be close to corresponding surface characteristics and intermediate between properties of the bulk solid and liquid phase. At $T = 1000 \text{ K}$, for the bulk solid Ni phase $D_{Ni}^{(s)} \cong 10^{-14} \text{ m}^2/\text{s}$ [28], for the bulk Ni melt $D_{Ni}^{(l)} \cong 10^{-9} \text{ m}^2/\text{s}$ [29]. The same order of magnitude was predicted in MD simulations [30] for Ni atoms in the Ni–Al melt. At $T = 1000 \text{ K}$, the coefficient of the self-diffusion on the surface of the bulk Ni phase is of order of $10^{-10} \text{ m}^2/\text{s}$ [31], i.e., of the same order of magnitude as the result of our above evaluation of D_i .

A visualization of the structure of NPs obtained by quenching is facilitated if the atoms of the components are represented not by spheres, but by points (Fig. 5). As can be seen from Fig. 5a, a polyicosahedral NP is formed as a result of quenching. Using the common analysis of a nearest neighbor search [32], it was revealed that the particle contains four nuclei of the icosahedral symmetry, three of which are shown in Fig. 5a with larger spheres (the fourth nucleus, which is located in the remote part of the particle, is not shown in Fig. 5a).

A more detailed analysis revealed that the nuclei have four axes of symmetry of the 5th order. In Fig. 5b, these axes are shown for three cores. Thus,

Table 1 Size dependence of the melting temperatures of single-component Ni and Al NPs: MD results

Metal	N	T_m (K)	
		EAM	TBP
Ni	1000	1315	1166
	2000	1366	1276
	3000	1403	1308
	5000	1452	1345
Al	1000	538	526
	2000	551	570
	3000	559	627
	5000	572	598

Figure 1 Images of the initial configurations of binary $\text{Ni}_{2500}\text{Al}_{2500}$ NPs with the uniform random distribution of components: **a** spherical NP, **b** cubic NP.

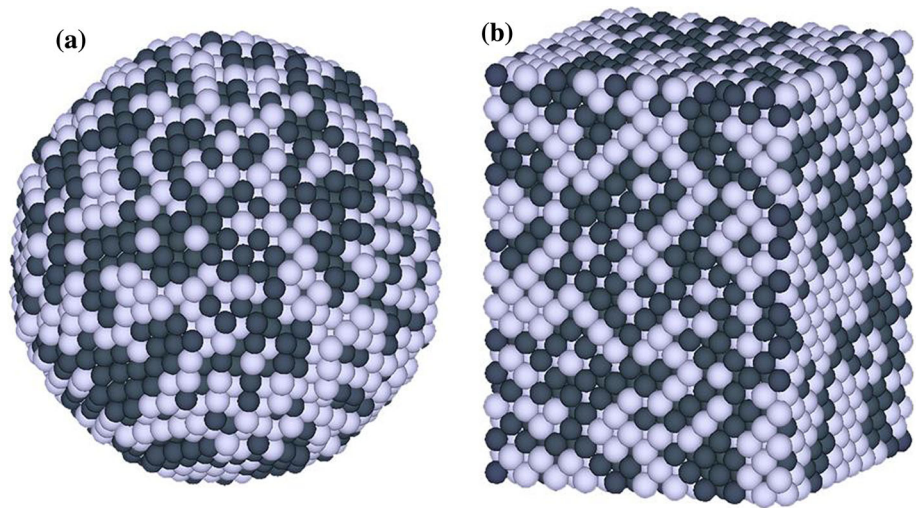


Figure 2 Snapshot (a) and central cross section (b) of a $\text{Ni}_{2500}@Al_{2500}$ bimetallic nanostructure obtained in our MD experiment by quenching for 50 ns a Ni–Al NP with an initial random distribution of components.

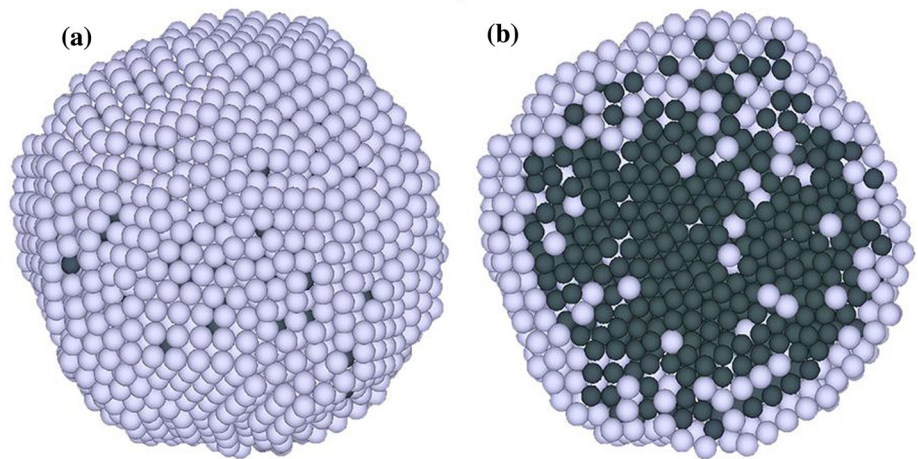
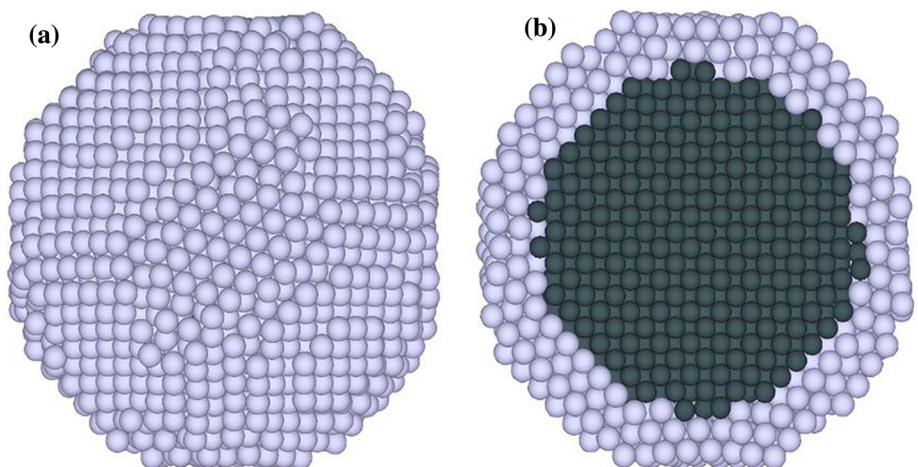


Figure 3 Snapshot (a) and central cross section (b) of a $\text{Ni}_{2500}@Al_{2500}$ nanostructure obtained by MD relaxation of a $\text{Ni}_{2500}@Al_{2500}$ NP in the form of the cut-off octahedron (fcc structure) for 10 ps.



the nanostructure shown in Figs. 2 and 5 can be interpreted as polyicosahedral with four cores having icosahedral symmetry (PolyIco-4).

In Fig. 6, the coloring of the atoms of the $\text{Ni}_{2500}@Al_{2500}$ NP corresponds to their energy spectrum: the dark blue color corresponds to the lowest and red color to the highest values of the potential (cohesive)

Figure 4 Snapshot (a) and central cross section (b) of a $\text{Ni}_{2500}@\text{Al}_{2500}$ nanostructure obtained by MD relaxation for 10 ps of a $\text{Ni}_{2500}@\text{Al}_{2500}$ NP of the icosahedral shape.

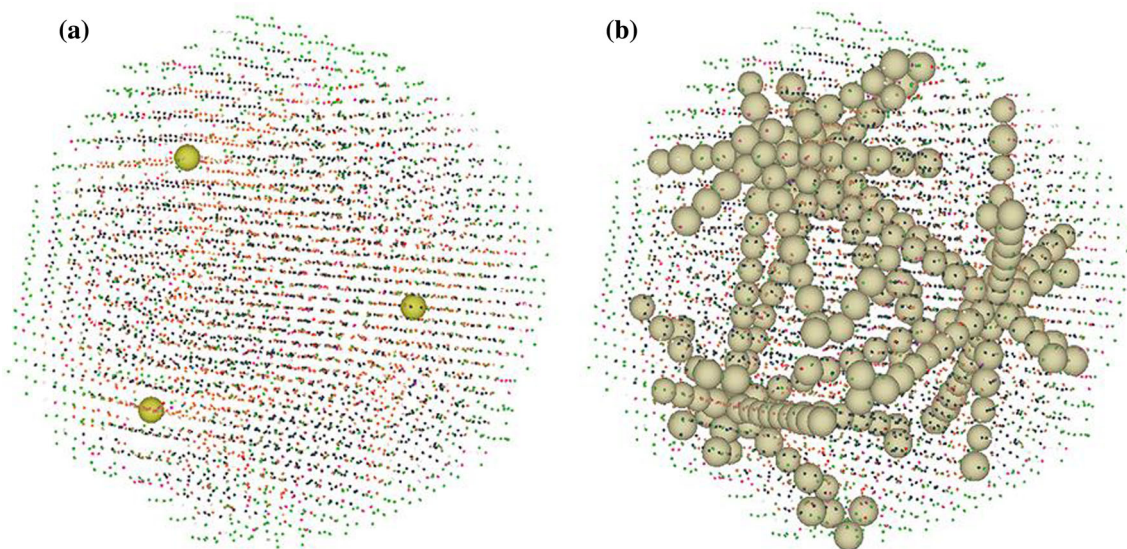
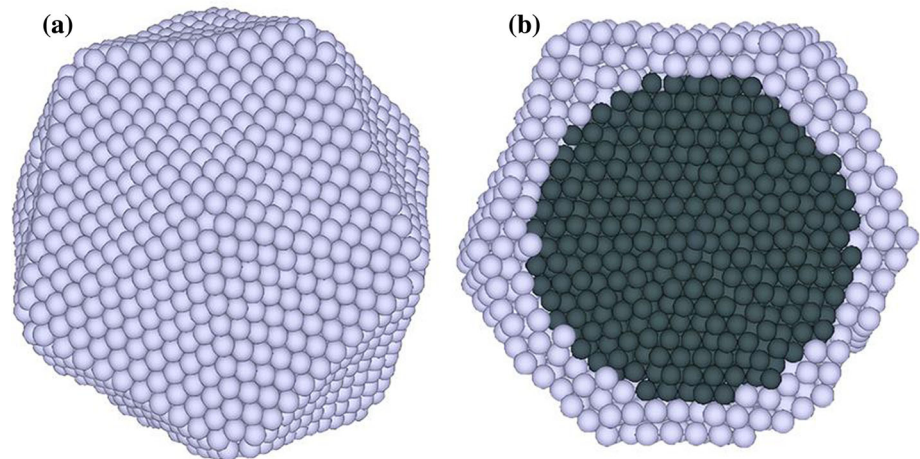


Figure 5 Polyicosahedral structure of a $\text{Ni}_{2500}@\text{Al}_{2500}$ NP obtained by quenching and shown in Fig. 2: a view of a nanoparticle with completely formed nuclei of icosahedral symmetry (a) and obtained fivefold symmetry axes (b).

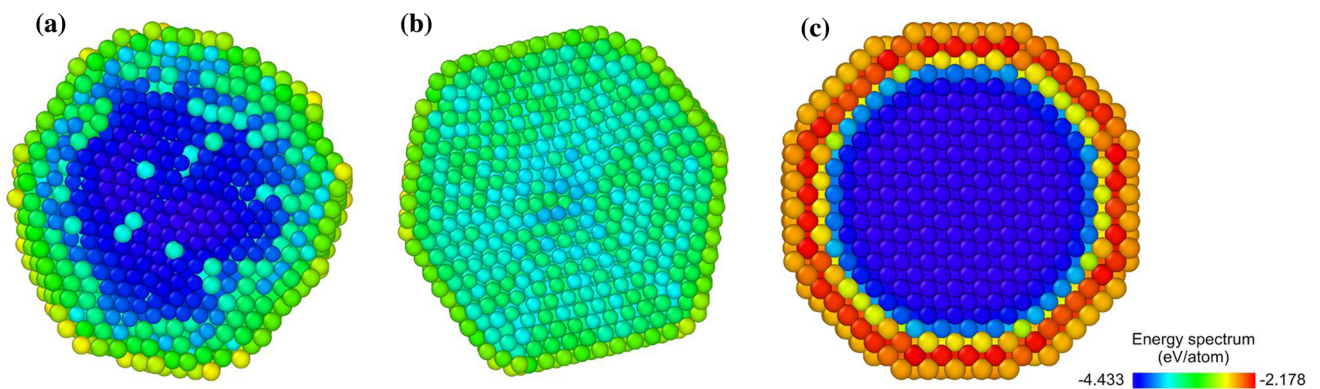


Figure 6 Equatorial cross sections of a $\text{Ni}_{2500}@\text{Al}_{2500}$ nanostructure with coloring of atoms corresponding to their energy spectrum: polyicosahedron obtained by quenching method (a), icosahedron (b) and truncated octahedron, i.e., fcc structure (c).

term u into the specific (per atom) internal energy. Here it is of particular significance that the polyicosahedron corresponds to the lowest values of u (Fig. 6a). The configuration shown in Fig. 6b corresponds to the relaxed icosahedral Ni@Al structure. The configurations shown in Fig. 6a and c differ markedly from Fig. 6 b in terms of their energy inhomogeneity. The values of the energies of Ni atoms in the core are close to the binding energy of the bulk Ni phase (4.435 eV [33]), while the energies of Al atoms in the shell correspond to the binding energy of the bulk Al phase (3.34 eV [33]). However, for the atoms of the outer monolayer of the shell, which are shown in red, the value of $u = -2.178$ eV/atom is more than 1 eV lower in modulus than the binding energy in bulk Al. Further discussion of the energy spectrum of Ni@Al nanostructures is presented in Sect. 4. In Table 2, the average quantitative characteristics of Ni@Al nanostructures are presented: the specific potential energy u , the volume V and the surface area S .

Results obtained by employing EAM

Using EAM, the process of hardening of Ni₂₅₀₀–Al₂₅₀₀ nanoparticles of equiatomic composition was simulated following to the same scheme as when using TBP. Figure 7 shows the configurations (images) of Ni–Al NPs following short-term relaxation at $T = 1000$ K for 10 ps (Fig. 7a) and after quenching at the cooling rate of 0.06 K/ps (Fig. 7b). The configurations shown in Figs. 7 a and b, which closely resemble each other, demonstrate evident segregation of Al atoms toward the surface of NPs: the outer monolayer consists entirely of Al atoms. Such evident surface segregation of Al in binary Ni–Al NPs is consistent with both the results of thermodynamic simulation [14] and the results presented in Sect. 3.1.

Table 2 Quantitative averaged characteristics of Ni₂₅₀₀@Al₂₅₀₀ nanostructures

Characteristic	Structure type Ni ₂₅₀₀ @Al ₂₅₀₀		
	Polyicosahedron	TO	PolyIco-4
u , eV/atom	– 3.722	– 3.395	– 3.469
S , nm ²	54	46	68
V , nm ³	72	64	88
S/V , nm ^{–1}	1.3	1.4	1.3

Figure 8 shows the central cross sections of a Ni₂₅₀₀Al₂₅₀₀ NP corresponding to the images shown in Figs. 7. It is shown in Fig. 8 that both Ni and Al atoms are present in the NP up to the outer monolayer consisting of Al atoms. In other words, the results of MD simulation using EAM predict the formation of Ni–Al@Al nanostructures rather than Ni@Al ones, in which the central part (core) is represented almost exclusively by Ni atoms. The configurations shown in Fig. 7 correspond to the NP of the initial spherical shape. If the choice of the initial configuration corresponds to a cubic NP (Fig. 1b), then already in 0.01 ns following the start of cooling, the cubic NP begins to “gutter” (Fig. 9a). By the time $t = 0.2$ ns (Fig. 9b), its shape becomes close to spherical, although signs of temporary (dynamic) faceting are still noticeable. However, the completion of quenching (Fig. 9c) corresponds to a spherical NP, whose appearance and structure do not significantly differ from the results corresponding to the quenching of spherical NPs.

Thus, all the following figures presented in this section correspond to the initial spherical shape of NPs. More detailed information about the core structure of Ni–Al@Al NPs and their surface layer can be obtained by analyzing the radial distributions of the local densities ρ_i of the components. Figure 10 demonstrates the density distributions of the components at $T = 1000$ K, i.e., following short-term relaxation for 10 ps, as well as distributions corresponding to the completion of quenching. The reduced density ρ_i^* was determined as the ratio of the local density $\rho_i(r)$ of the components to the density $\bar{\rho}_i$ averaged over the volume of the NP. Here, the absence of segregation (uniform distribution of components) would correspond to $\rho_{Ni}^* = \rho_{Al}^* = 1$. Figure 10 confirms the earlier conclusion that significant structural rearrangements already occurring in NPs in the process of the initial relaxation at $T = 1000$ K are the cause of the evident segregation of components: the outer monolayer is represented by Al atoms, the second (inner) monolayer—by Ni atoms, while the central area of NPs contain atoms of both types, albeit with Ni atoms predominating. Quenching leads to a noticeable increase in the concentration of Al atoms in the first (outer) monolayer and an increase in the concentration of Ni atoms in the second (inner) monolayer.

Figure 7 Snapshots of a $\text{Ni}_{2500}\text{Al}_{2500}$ NPs after relaxation at $T=1000$ K for 10 ps (a) and after subsequent quenching at the cooling rate of 0.06 K/ps (b).

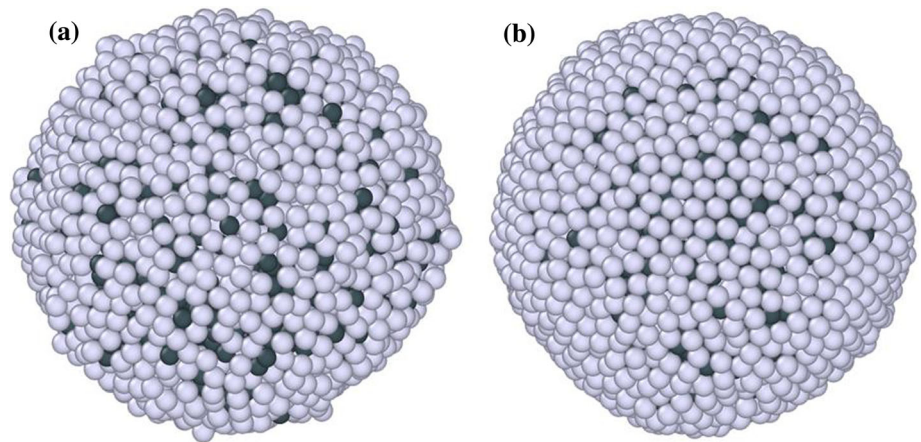


Figure 8 Central cross sections of the $\text{Ni}_{2500}\text{Al}_{2500}$ NP corresponding to the snapshots shown in Figs. 7 at 1000 K (a) and at 0.01 K (b).

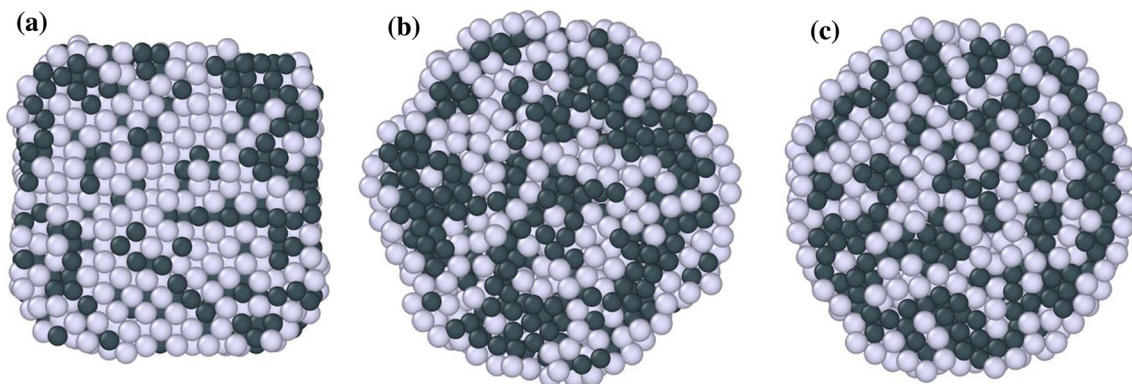
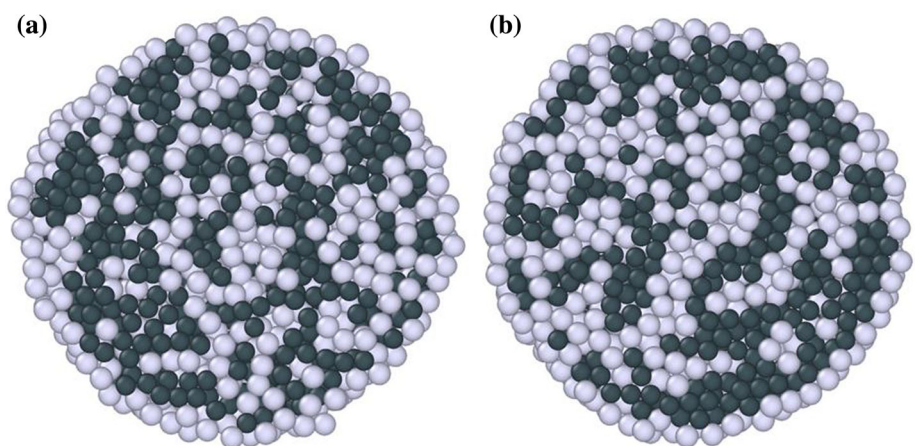


Figure 9 Central cross sections of the NP having an initial cubic shape by different quenching times: $t=0.01$ ns (a), $t=0.2$ ns (b), and $t=16.6$ ns (c). The rate of cooling from $T=1000$ K to $T=0.01$ K was 0.06 K/ps.

Instead of the reduced densities of the components ρ_i^* , one can consider the local molar fractions of the components to be represented by

$$x_{\text{Ni}} = \rho_{\text{Ni}}^*/(\rho_{\text{Ni}}^* + \rho_{\text{Al}}^*) \text{ and } x_{\text{Cu}} = \rho_{\text{Cu}}^*/(\rho_{\text{Ni}}^* + \rho_{\text{Al}}^*).$$

Thus, the molar fractions of the components $x_i^{(c)}$ in the core of the NP can also be estimated. According to our estimates, $x_{\text{Ni}}^{(c)} \approx 0.6$, $x_{\text{Al}}^{(c)} \approx 0.4$. In the cooling curve, i.e., in the temperature dependence of the potential term into the specific internal energy, an angular break is demonstrated at a temperature $T \approx$

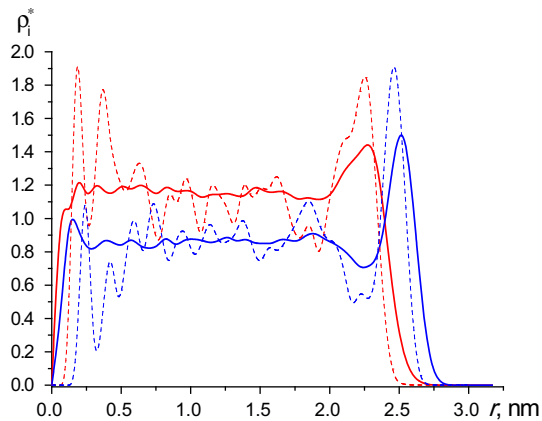


Figure 10 Radial distributions of the reduced local densities of the components of Ni–Al NPs after the short-term relaxation for 10 ps at $T=1000$ K (solid curves) and after completion of quenching at temperature of 0.01 K (dashed curves). Distributions for Ni are shown by red curves and distributions for Al by blue lines.

500 K (Fig. 11). A discussion on the physical nature of this effect is presented in Sect. 4.

Discussion

Thus, the possibility of obtaining ordered core-shell nanostructures by quenching Ni–Al NPs is confirmed by the results of our MD simulations using two different interatomic interaction potentials: TBP and an EAM potential. The results obtained using TBP correspond to the formation of Ni@Al nanostructures with almost perfectly segregated components, i.e., core-shell nanostructures of the commonly

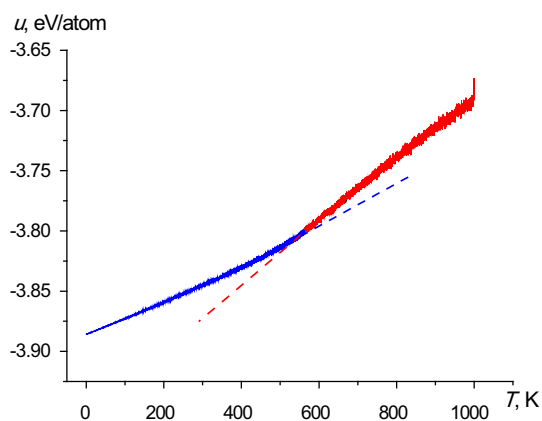


Figure 11 The temperature dependence of the specific potential energy of $\text{Ni}_{2500}\text{Al}_{2500}$ NPs in the course of their quenching, i.e., cooling from 1000 K to 0.01 K for 16.6 ns.

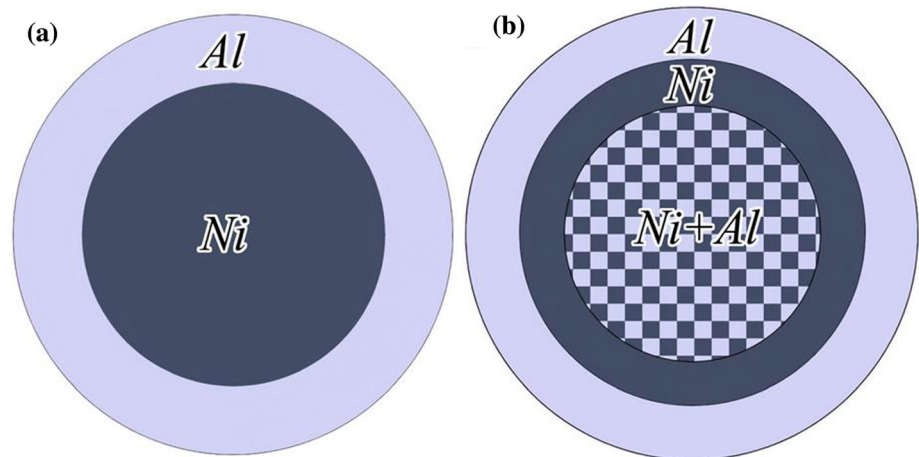
considered type (Fig. 12a). In MD simulations using EAM, the result of quenching was core-shell nanostructures of a more complex type, shown schematically in Fig. 12b.

Obviously, the main factor determining the possibility of spontaneous (under controlled self-assembly) formation of core-shell nanostructures is the surface segregation of one of the components. In other words, this consists of the tendency toward the spontaneous surface segregation of Al in binary Ni–Al NPs, which is confirmed by MD results and the results of thermodynamic simulation [14]. However, this surface segregation is highly dependent on temperature. Thermodynamics [34] predicts a decrease in the surface segregation with increasing temperature; this trend is especially noticeable when going from solid NPs to nanodroplets. However, as the temperature decreases, the role of kinetic factors increases. Therefore, even NPs—i.e., small objects—may not reach the equilibrium or quasi-equilibrium state corresponding to a noticeable surface segregation predicted by equilibrium thermodynamics. Accordingly, it can be concluded that the initial temperature and cooling rate, which are directly related to the cooling time from the initial temperature T_0 to the final temperature T_f , should act as the main parameters to determine the quenching result.

Although the initial chosen temperature $T_0=1000$ K is lower than the melting temperature of Ni NPs of the same size as binary NPs, it is higher than the melting temperature of Al NPs (Table 1). Obviously, such a choice of the initial temperature provides the necessary conditions for the segregation process to occur on time scales that can be reproduced in MD experiments. Heating of Al@Ni NPs was simulated in [10] starting from $T_0 = 300$ K. As a result, a V-shaped curve with a minimum at $T = 1000$ K was found in the temperature dependence of the specific potential energy $u(T)$. This dependence may be explained in terms of the destruction of the energetically unfavorable Al@Ni nanostructure. The authors of [10] explained the V-shaped dependence in terms of the synergy between the mixing effect and disordering effect during continuous heating.

When quenching, i.e., upon cooling Ni–Al NPs with initially uniform distribution of components, the $u(T)$ dependence shown in Fig. 11 demonstrates a kink, i.e., a transition from one linear segment to another, which corresponds to a smaller value of the

Figure 12 Two types of core-shell nanostructures corresponding to MD simulations using TBP (a), and EAM (b).



slope coefficient $K = du/dT$. Segment 1 corresponds to $K_1 = 0.00027$ eV/K; the second segment—to $K_2 = 0.00015$ eV/K. In our opinion, this effect is explained by crystallization in the outer Al monolayer, i.e., the disappearance of the surface melting effect. If we assume that structural changes at $T = 500$ K take place only in the outer monolayer, then the difference $K_1 - K_2$ should correspond to the difference Δc of the specific heat capacities of Al in the liquid c_L and solid c_S states:

$$\Delta c = c_L - c_S = K_1 - K_2 = 0.00012 \text{ eV/K.}$$

Turning to the molar heat capacities, was found that $\Delta C = 11.6$ J/mol K. The obtained value agrees satisfactorily with the difference 7.7 J/mol K in the heat capacities of aluminum in the liquid (31.86 J/mol K) and solid (24.2 J/mol K) states [27].

The results of MD simulation using the TBP were subjected to a more detailed analysis of the structural transformations occurring during quenching. In particular, it was found that the result of quenching is the formation of Ni–Al NPs having a polyhedral structure, i.e., having several fully formed nuclei of icosahedral symmetry (Fig. 5). However, questions remained open about how close these nanostructures are to the equilibrium state and whether they are more stable than Ni@Al nanostructures in icosahedron (Ico) (Fig. 6b) and truncated octahedron (TO) form (Fig. 6c).

Structural relaxation processes in NPs can occur for characteristic times of order of 1 s and even in the order of 1 h. Although such relaxation times are obviously inaccessible for reproduction in MD experiments, in order to understand the directions of evolution of nanostructures on time scales beyond the limits of MD capabilities, it is possible to use

approaches related to the optimization of nanostructures as a result of MD evolution. In the present work, we used an approach that corresponds to a step-by-step replacement of atoms of various sorts with the selection of configurations corresponding to a decrease in the potential energy of the nanostructures being optimized. Although this kind of optimization has been used earlier [25], the presented approach to interpreting the results of such kind of optimization appears to be novel. Figure 13 shows configurations of NPs resulting from the optimization of the nanostructures shown in Fig. 6.

By comparing Figs. 6 and 13, we can conclude that the optimization procedure leads to a noticeable redistribution of atoms in terms of their energies. In particular, there is a noticeable decrease in the atomic energies in the two outer monolayers of polyicosahedral NPs (Fig. 13a). However, the results presented in Table 3 are more interesting; here, in addition to the potential term into the specific internal energy, the surface area of NPs, S and their volume V , the differences Δu , ΔS and ΔV between the values of the corresponding quantities both before and after the optimization under discussion are also presented. Here it can be seen that the polyhedral nanostructure obtained by quenching is characterized by the smallest values of the differences Δu , ΔS , and ΔV . Thus, this nanostructure should be the closest to equilibrium and, consequently, the most stable.

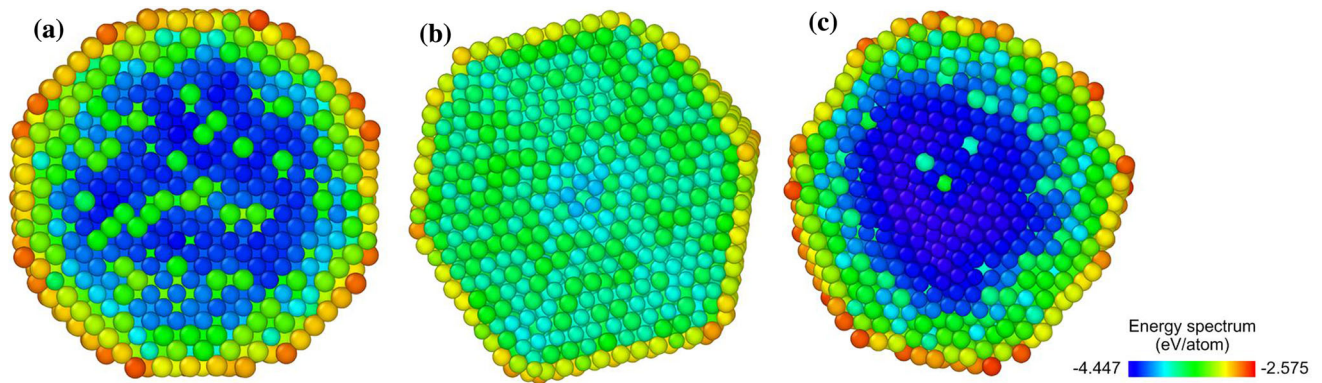


Figure 13 Equatorial cross sections of bimetallic NiAl NPs after optimization by interchanging of sorts: PolyIco-4 configuration obtained by quenching (a), Ico (b), fcc nanocrystal in the shape of TO (c).

Table 3 Comparison of parameters of non-optimized and optimized configurations

Characteristic	Type of nanoparticle		
	PolyIco-4	TO	Ico
μ , eV/atom	- 3.730	- 3.648	- 3.549
$\Delta\mu$, eV/atom	- 0.08	- 0.256	- 0.08
S , nm ²	72	66	83
ΔS , nm ²	0	2	- 5
V , nm ³	55	49	62
ΔV , nm ³	1	3	- 6

Conclusions

The MD results presented in this work, which were obtained using both TBP and EAM, show that bimetallic nanostructures having a shell of Al atoms can be formed as a result of rapid cooling (quenching). At the same time, MD simulations using TBP predict the formation of the commonly considered type of Ni@Al nanostructures having almost completely separated components, while the central area (core) of the more complex NiAl@Ni@Al nanostructures obtained using EAM is represented by atoms of both metals, but with a predominant Ni content. However, in this case, the outer monolayer of NPs also consists only of Al atoms. In the inner subshell (second and third monolayers), as shown in Figs. 8b, 9b and 10, only a small fraction of Al atoms is present.

The initial temperature T_0 and cooling rate $|dT/dt|$ at quenching may be considered as two main factors affecting dynamics of segregation and the result of the quenching process. The initial temperature of

1000 K provides a sufficiently high rate of structural rearrangements in Ni–Al NPs with an initially homogeneous distribution of components. Indeed, already after a short-term relaxation, a noticeable redistribution of components in the initial NPs occurs, while upon quenching, the segregation process is completed. Selecting a higher temperature would decrease the surface segregation effect during the annealing stage, while a lower temperature would slow down the segregation process at both annealing and quenching stages.

Strictly speaking, at a temperature of the order of 0.01 K corresponding to the final temperature T_f of quenching, the classical MD is inapplicable. However, in our case, $T_f = 0.01$ K was used as some conditional limiting value corresponding to the almost complete exclusion of the thermal motion of atoms. As a result, practically identical final nanostructures are obtained at $T_f = 100$ K. Along with T_0 , an important parameter of the hardening process is the cooling rate dT/dt . At $|dT/dt| = 0.06$ K/ps, quenching significantly increases the degree segregation of components. A further decrease in the cooling rate to $|dT/dt| = 0.01$ K/ps has almost no effect on the quenching results. However, at a higher cooling rate of order of 1 K/ps, the quenching effect practically disappears.

On the basis of the MD simulation results, it is difficult to conclude which of the two alternative Ni@Al or NiAl@Ni@Al nanostructures should be observed in direct experiments on the quenching of Ni–Al NPs. Perhaps, due to some factors not taken into account in the MD experiments, the formation of bimetallic nanostructures of both types is possible. Evidently, factors promoting the self-assembly of

core-shell nanostructures may include the spontaneous segregation of one of the components, optimal values of the annealing temperature and the quenching rate. These factors should determine the final structure of bimetallic NPs obtained not only by quenching binary NPs with an initial uniform distribution of components, but also the structures of bimetallic NPs obtained by other methods, for example, by condensation from the gas phase or by the EEW method. In any case, the probability of forming bimetallic NPs having a shell of Al atoms should significantly exceed the formation probability of nanostructures having a shell of Ni atoms. Obviously, the patterns found in our MD experiments may be applied not only to Ni–Al NPs, but also to other binary nanoalloys where there is a pronounced segregation of one of the components.

Acknowledgements

The research was carried out with the financial support of the Russian Foundation for Basic Research (project no. 20-33-90192), as well as the Ministry of Education and Science of the Russian Federation as part of the state task in the field of scientific activity (project no. 0817-2020-0007).

Authors contribution

SB: investigation, visualization, methodology. VS: conceptualization, methodology, writing original draft, review and editing. NS: supervision, conceptualization, writing original draft, review and editing. VM: software, methodology. IT: investigation, formal analysis, data curation. KS: investigation, formal analysis, resources. VR: formal analysis, data curation, review and editing, AK: validation, investigation, data curation.

Funding

The authors received no funding from any source.

Data availability

All data, models, and code generated or used during the study appear in the submitted article.

Declarations

Conflict of interest The authors declare no competing interest with any previous work.

Consent to participate Not applicable.

Consent for publication Not applicable.

Ethical approval Not applicable.

Appendix: Additional information on involved interatomic potentials

The tight binding potential can be presented by the next analytical expression [20]

$$U = \sum_{i=1}^N \left\{ \sum_{j \neq i}^N A \exp \left(-p \left(\frac{r_{ij}}{r_0} - 1 \right) \right) - \left[\sum_{j \neq i}^N \zeta^2 \exp \left(-2q \left(\frac{r_{ij}}{r_0} - 1 \right) \right) \right]^{1/2} \right\}$$

for the potential term U into the internal energy of a metal system consisting of N atoms. Here r_{ij} is the distance between atoms i and j , r_0 is the distance between the nearest neighbors (for fcc metals $r_0 = a/\sqrt{2}$, a is the lattice parameter), A, ζ, p, q are variable parameters selected according to chosen experimental values of the cohesion energy, the lattice parameter (taking into account the limitation on the atomic volume) and independent elastic constants in the corresponding crystal structure at a temperature $T = 0$ K. The cross parameters for the tight binding potential were determined using the Lorentz-Berthelot rule, i.e., the parameters A and ζ were found as geometric means whereas p, q and r_0 as arithmetic means. Table 4 shows both parameters for Ni and Al [20] as well as the calculated values of the cross parameters for the Ni–Al system. Such a

Table 4 Parameters of the tight binding potential

Metal	A (eV)	ζ (eV)	p	q	r_0 (Å)
Ni [20]	0.0376	1.070	16.9988	1.189	2.4918
Al [20]	0.1221	1.316	8.612	2.516	2.8634
Ni–Al	0.06785	1.18665	12.8053	1.8525	2.6776

scheme was tested by us in [24, 25] for the Ni based bimetallic nanoparticles.

In the frames of the basic embedded atom method (EAM) [35], the total potential energy U of a metal body is presented as follows:

$$U = \sum_i F_i(\rho_{h,i}) + \frac{1}{2} \sum_i \sum_{j(\neq i)} \varphi(r_{ij})$$

where $F_i(\rho_{h,i})$ is the embedding function; i.e., the energy necessary to embed an atom into a point with the electron density $\rho_{h,i}$ and $\varphi(r_{ij})$ is the core-core (repulsion) pair potential for two atoms separated by distance r_{ij} . The whole local electron density $\rho_{h,i} = \sum_{j(\neq i)} \rho_j^a(r_{ij})$ is calculated as the superposition of the atomic contributions. So, for practical applications of EAM, the embedding function $F_i(\rho_{h,i})$ and the repulsion potential $\varphi(r_{ij})$ should be found. In [21] sets of the EAM parameters are proposed and verified for 12 metals including Ni and Al. Besides, an algorithm was developed and verified which makes it possible to generate a cross potential for any alloy of these metals. The EAM potentials [21] for Ni and Al are tabulated on site [36] in a format available for open and well-verified program LAMMPS [37] which makes it possible to perform parallel calculations employing the graphical processing units. A program for generation of cross potentials for alloys following the mentioned above algorithm may be also found on site [36].

References

- [1] Taylor TA, Overs MP, Quets JM, Tucker RC (1983) Development of several new nickel aluminide and chromium carbide coatings for use in high temperature nuclear reactors. *Thin Solid Films* 107:427–435
- [2] White CL, Padgett RA, Lin CT, Yalisove SM (1984) Surface and grain boundary segregation in relation to intergranular fracture: boron and sulfur in Ni₃Al. *Scr Metall* 18:1417–1420
- [3] Takasugi T, George EP, Pope DP, Izumi O (1985) Intergranular fracture and grain boundary chemistry of Ni₃Al and Ni₃Si. *Scr Metall* 19:551–556
- [4] Okamoto H (1993) Al-Ni (Aluminum – Nickel). *J Phase Equilibria* 14:257–259
- [5] Le Y, Juan H, Xiaolong W, Zhang Q, Deng L (2016) Galvanic displacement synthesis of Al/Ni core-shell pigments and their low infrared emissivity application. *J Alloys Compd* 670:275–280
- [6] Klein T, Pauly Ch, Mücklich F, Kiuckelbick G (2020) Al and Ni nanoparticles as precursors for Ni aluminides. *Intermetallics* 124:106839
- [7] Cui H-Z, Wei N, Zeng L-L, Wang X-B, Tang H-J (2013) Microstructure and formation mechanism of Ni-Al intermetallic compounds fabricated by reaction synthesis. *Trans Nonferrous Met Soc China* 23:1639–1645
- [8] Lebrat JP, Varma A (1993) Self-propagating high-temperature synthesis of Ni₃Al. *Combust Sci Technol* 88:211–222
- [9] Babuk VA, Vassiliev VA, Sviridov VV (2001) Propellant formulation factors and metal agglomeration in combustion of aluminized solid rocket propellant. *Combust Sci Technol* 163:261–289
- [10] Song P, Wen D (2010) Molecular dynamics simulation of a core-shell structured nanoparticle. *J Phys Chem C* 114:8688–8696
- [11] Kart SO, Kart HH, Cagin T (2020) Atomic-scale insights into structural and thermodynamic stability of spherical Al@Ni and Ni@Al core-shell nanoparticles. *J Nanopart Res* 22:140
- [12] Samsonov VM, Talyzin IV, Yu KA, Vasiliyev SA (2019) Surface segregation in binary Cu–Ni and Au–Co nanoalloys and the core-shell structure stability/instability: thermodynamic and atomistic simulations. *Appl Nanosci* 9:119–133
- [13] Yu SN, Samsonov VM, Yu KA, Vasilyev SA, Myasnichenko VS, Sokolov DN, Savina KG, Veselov AD (2019) To the problem of stability/instability of bimetallic structures Co (Core)/ Au (Shell) and Au (Core)/ Co (Shell): atomistic simulation. *Phys Chem Asp Study Clust Nanostr Nanomat* 11:520–534
- [14] Samsonov VM, Talyzin IV, Yu KA, Vasiliyev SA, Alymov MI (2021) On the problem of stability/instability of bimetallic core-shell nanostructures: molecular dynamics and thermodynamic simulation. *Comput Mater Sci* 199:110710
- [15] Eom N, Messing ME, Johnson J, Deppert K (2021) General trends in core-shell preferences for bimetallic nanoparticles. *ACS Nano* 15:8883–8885
- [16] Akbarzadeh H, Mehrjouci E, Abbaspour M, Shamkhali AN (2021) Melting behavior of bimetallic and trimetallic nanoparticles: a review of MD simulation studies. *Top Curr Chem* 379:22
- [17] Liao H, Fisher A, Xu ZJ (2015) Surface segregation in bimetallic nanoparticles: a critical issue in electrocatalyst engineering. *Small* 11:3221–3246
- [18] Saleem F, Cui X, Zhang Z, Liu Z, Dong J, Chen B, Chen Y, Cheng H, Zhang X, Ding F, Zhan H (2019) Size-dependent

- phase transformation of noble metal nanomaterials. *Small* 15:1903253
- [19] Pervikov A, Lozhkomoiev A, Bakina O, Lerner M (2019) Synthesis of core-shell and janus-like nanoparticles by non-synchronous electrical explosion of two intertwined wires form immiscible metals. *Solid State Sci* 87:146–149
- [20] Cleri F, Rosato V (1993) Tight-binding potentials for transition metals and alloys. *Phys Rev B* 48:22–33
- [21] Zhou XW, Johnson RA, Wadley NG (2004) Misfit-energy dislocations in vapor-deposited CoFe/NiFe multilayers. *Phys Rev B* 69:144113
- [22] Samsonov VM, Yu SN, Myasnichenko VS, Talyzin IV, Kulagin VV, Vasilyev SA, Bembel AG, Yu KA, Sokolov DN (2018) A comparative analysis of the size dependence of the melting and crystallization temperatures in silver nanoparticles via the molecular dynamics and monte-carlo methods. *J Surf Invest X-ray, Synchrotron Neutron Tech* 12:1206–1209
- [23] Samsonov VM, Yu SN, Yu KA, Talyzin IV, Yu KA, Vasilyev SA, Myasnichenko VS, Sokolov DN, Savina KG, Veselov AD, Bogdanov SS (2021) Factors of the stability/instability of bimetallic core-shell nanostructures. *Bull Russ Acad Sci Phys* 85:950–954
- [24] Sdobnyakov N, Khort A, Myasnichenko V, Podbolotov K, Romanovskaia E, Kolosov A, Sokolov D, Romanovski V (2020) Solution combustion synthesis and monte carlo simulation of the formation of CuNi integrated nanoparticles. *Comput Mater Sci* 184:109936
- [25] Romanovskii VI, Yu KA, Khort AA, Myasnichenko VS, Podbolotov KB, Savina KG, Sokolov DN, Romanovskaia EV, Yu SN (2020) Features of Cu – Ni nanoparticle synthesis: experiment and computer simulation. *Phys Chem Asp Study Clust Nanostr Nanomat* 12:293–309
- [26] Paz Borbón LO (2011) Computational studies of transition metal nanoalloys. Doctoral thesis accepted by University of Birmingham. Springer-Verlag, Berlin, Heidelberg
- [27] Mills KC (2002) Recommended values of the thermophysical properties of eight alloys, 1st edn. Woodhead Publishing Ltd, Cambridge
- [28] Adda Y, Philibert J (1999) *La diffusion dans les Solids*, vol 2. Universitaires de France, Paris
- [29] Meyer A (2015) The measurement of self-diffusion coefficients in liquid metals with quasielastic neutron. *Scatt EPJ Web of Conf* 83:01002
- [30] Cao Q-L, Tu F, Xue L, Wang F-H (2019) Assessing relationships between selfdiffusion coefficient and viscosity in Ni-Al alloys based on the pair distribution function. *J Appl Phys* 126:105108
- [31] Bonzel HP (1990) Surface diffusion tables. In: Mehrer H (ed) *Landolt-börnstein group III: condensed matter*, vol 26. Diffusion in solid metals and alloys. Springer, Berlin, pp 728–733
- [32] Stukowski A (2010) Visualization and analysis of atomistic simulation data with OVITO – the open visualization tool. *Model Simul Mater Sci Eng* 18:015012
- [33] Kittel Ch (2004) *Introduction to solid state physics*, 8th edn. Wiley
- [34] Kaptay G (2016) Modeling equilibrium grain boundary segregation, grain boundary energy and grain boundary segregation transition by the extended butler equation. *J Mater Sci* 51:1738–1755. <https://doi.org/10.1007/s10853-015-9533-8>
- [35] Daw MS, Baskes MI (1984) Embedded-atom method: derivation and application to impurities, surfaces, and other defects in metals. *Phys Rev B* 29:6443–6453
- [36] Interatomic Potentials Repository <https://www.ctcms.nist.gov/potentials>. Accessed 10 Mar 2022
- [37] LAMMPS Molecular Dynamics Simulator. <https://www.lammps.org>. Accessed 10 Mar 2022

Publisher's Note Springer Nature remains neutral with regard to jurisdictional claims in published maps and institutional affiliations.